FREE ELECTRON LASERS

The free-electron laser (FEL) is a device that uses part of the kinetic energy of nearly-free electrons (not bound in atoms or in condensed matter) to generate coherent electromagnetic radiation, see Refs. 1–3. The electrons are supplied in the form of a beam accelerated to relativistic velocities. The electron beam can either pass through the gain medium only once, or be recycled in a storage ring, which can then allow the electrons to circulate many times through the FEL. Electrons are not entirely free: as will be explained here, free electrons cannot interact efficiently with radiation in vacuum.

Thus, they will interact with radiation in two types of structures: (1) a device in which electrons are accelerated in an inhomogeneous (periodic) magnetic or electromagnetic field, called a wiggler or an undulator; and (2) a device in which electrons are unperturbed but the laser wave is subject to dispersion (as in Čerenkov transition radiation or Smith-Purcell devices). Because the FEL is a laser, it is based on stimulated emission in which radiation is mostly emitted coherently, that is, with the same phase as already existing radiation. For this, the interaction region is enclosed in a laser cavity (see CAVITY RESONATORS) to allow the emitted light to be fed back and to stimulate further emission. If the light passes many times through the gain medium, FEL can operate even in a small-gain regime. Because mirrors with sufficient reflectivity are not available for the ultraviolet (UV) and shorter wavelength range, FELs in this range are designed without mirrors on the principle of amplified spontaneous emission, such that radiation from one part of the electron beam or an injected signal stimulates radiation from other parts, passing them only one time. The large-gain regime of a FEL is necessary for this kind of operation (4). Sometimes SPONTANEOUS EMISSION of free electrons is used (termed indulator radiation) (5).

Let us consider, as an example, a FEL with a static magnetic wiggler (Fig. 1). The laser has frequency ν and wavelength λ_L with the corresponding wavevector $k_L = 2\pi/\lambda_L$. The wiggler has spatial period λ_W and wavevector $k_W = 2\pi/\lambda_L$. Then the combined wave of the laser and the wiggler field (called "ponderomotive potential") has the phase $(k_L + k_W)z - \nu t$. In order to interact with a permanent rather than an oscillating force, the electron must maintain constant phase relative to the ponderomotive potential. This is called "synchronism condition." Then the electron must have a velocity approaching the "resonant velocity"

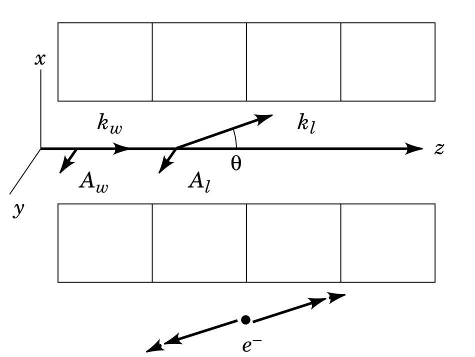

Figure 1. Schematic of the wiggler and laser fields (top), and the momentum change in the processes of emission and absorption (bottom).

$$v_r = \frac{\nu}{k_L + k_w} \tag{1}$$

Without a wiggler ($k_w = 0$) in vacuum ($\nu = k_L c$) the resonant velocity is equal to the speed of light c, unattainable by electrons. Due to the presence of a wiggler or of a refractive index, the resonant velocity is less than the speed of light and the laser operation is then possible.

Perhaps the most salient feature of FELs is their tunability. Velocity v of the electron (with mass m) is related to its energy $E = \gamma mc^2$ via the Lorentz factor $\gamma = (1 - (v/c)^2)^{-1/2}$. Definition of the resonant velocity from Eq. (1) results a rough determination of the wavelength of the laser

$$\lambda_L = \frac{\lambda_W(1 + a_w^2)}{2\gamma^2} \tag{2}$$

where a_w is a parameter depending on the wiggler field (see below), usually of the order of unity. Electron energy from MeV to GeV corresponds to Lorentz factors ranging from approximately 2 to 2000. For the wiggler period of the order of a centimeter laser radiation can, in principle, have a wavelength that ranges from microwave to hard X-ray. Another important feature of FELs is their ability to yield large peak power, which scales up with the electron peak current, up to hundreds of amperes for electron pulses produced by present-day accelerators. On the other hand, average power output is much lower.

The FEL was first proposed on the basis of quantum electrodynamics (6). It was later understood that, for FELs emitting in the visible and shorter-wavelength range, quantum effects play a negligible role and their operation could be explained within a classical theory (7,8).

In the quantum description (9), FELs owe their gain to the fact that an electron recoils in opposite directions, depending on whether it emits or absorbs a photon with a given wavevector k_L; hence, the resonant electronic momentum $\hbar k_{er}$ for the emission of such a photon differs from the resonant momentum $\hbar k_{ar}$ for its absorption. Probabilities of emission and absorption of a photon as functions of the initial electron momentum (lineshapes) are centered at k_{er} and k_{ar}, respectively [Fig. 2(a)]. Spontaneous emission has the same lineshape as stimulated emission. The quasiclassical limit holds when k_{er}–k_{ar} is much smaller than the inverse length of the wiggler, and the photon energy $\hbar c k_L$ is much smaller than the electron energies $E(k_{e(a)r})$. In this limit, the gain curve is antisymmetric about the mean resonant momentum $k\hbar = \hbar(k_{er} + k_{ar})/2$ [see Fig. 2(b)], which corresponds to resonant velocity v_r. In this limit, the quantum expression for gain coincides with its classical counterpart.

In the classical description (1–3), the wiggler field will periodically deflect the electrons perpendicular to their direction of travel (along the wiggler axis). The small-gain regime occurs whenever it is possible to neglect the amplification of the field when considering the motion of electrons. In this limit, the oscillations of the electrons in the ponderomotive poten-

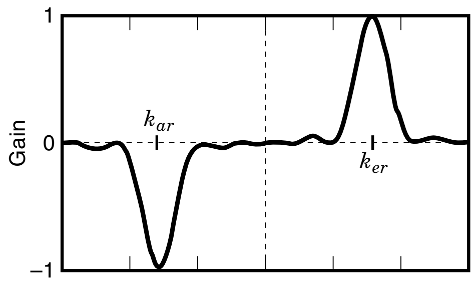

(**a**)

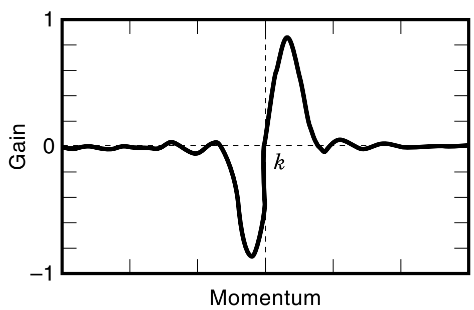

(**b**)

Figure 2. Gain in a FEL for large recoil results from resolved profiles of emission and absorption (a). For small recoil, gain is the difference of overlapping emission and absorption and is antisymmetric.

tial are described by the pendulum equation. It turns out that in such a potential electrons having a velocity higher than v_r on the average give energy to the laser, thus contributing to gain; electrons having a velocity lower than v_r absorb the energy from the laser, thus contributing to loss. This results in a gain curve, as in Fig. 2(b), which we designate G_{st}.

The combined effect of the wiggler field and the laser field, i.e., the ponderomotive potential, causes "axial bunching" of the electrons. The electrons injected at random times are forced into periodically spaced bunches separated by approximately the laser wavelength. This bunching is associated with the gain or loss of energy by electrons, or, equivalently, their axial acceleration or deceleration, depending on the phase between their transverse motion and the laser wave. If bunching is significant, so is the change of both laser field amplitude and phase. This change promotes further bunching. This process is a rare example of useful instability. As a result of their bunching, electrons radiate in-phase and their emitted fields add up coherently, so that the total emitted intensity is proportional to the electron current squared, rather than being proportional to the current, as in the case of randomly distributed electrons. When the radiation of electrons is essentially collective, this is called a "large-gain regime." In this large-gain regime, the gain lineshape is no longer antisymmetric.

The first FEL (10) was operated in 1977. A variety of FELs (1–3) now operate successfully over a spectral range of from millimeter- down to ultraviolet wavelengths. On the other hand, FEL operation in the X-ray and extreme ultraviolet (XUV) domains (11) is still facing considerable difficulties, primarily because of the stringent requirements FEL poses on the allowed electron beam energy spread and emittance. (The beam emittance is the product of the transverse size of the beam and the velocity angle spread.) These requirements stem from the antisymmetric dependence on the small-gain standard gain G_{st} being dependent upon the deviation of the electron velocity v from the resonant velocity v_r. [This is related to the Madey theorem, which states that gain lineshape is proportional to the derivative of the spontaneous emission lineshape over the velocity (12)]. Electrons initially below resonance contribute to absorption and electrons above resonance contribute to emission. Therefore this gain lineshape allows for net gain only if the initial momentum distribution is centered above v_r, which we call momentum population inversion. It also restricts the momentum spread, at which gain is significant, to values comparable to the width of the positive (gain) part of G_{st}. This width decreases significantly with laser wavelength, thereby limiting severely FEL gain performance at short wavelengths.

A variation of a FEL having two wigglers and a drift region between them (called *optical klystron*) was realized (13). In this device, the first wiggler serves to "bunch" the electron phases, which then acquire favorable values in the drift region between the wigglers, and finally yield enhanced gain in the second wiggler. Its gain lineshape has a higher maximum value, which is an advantage for electron beams with small energy spread. However, the width of the gain region is proportionally narrower, which makes the restrictions for the energy spread even more severe.

In search of shorter-wavelength sources, researchers considered the stimulated Čerenkov radiation by quasi-free electrons in a refracting medium, or Čerenkov transition radiation (TR) in a periodic dielectric structure, see Refs. 14,15. The Čerenkov TR can exist even above the plasma frequency (corresponding to $\sim$30 eV) where the refractive index $n < 1$ and the usual Čerenkov effect is impossible, because TR occurs when an electron crosses a boundary between different refractive indices. In a structure with a spatially periodic index of refraction, the Čerenkov effect results from the constructive interference of TR from different layers. The period of these layers (which plays the role of k_W) can be shortened much more than in magnetostatic wigglers. The pursuit of shorter wavelengths has also led to the proposal of a FEL in which the magnetostatic wiggler is replaced by an intense electromagnetic wave (the Compton-scattering FEL) (11,16). Its wavelength ($\lambda_w \sim 1$ μm and thus $\lambda_L \sim 1$ nm) would be much shorter than in existing lasers. In all of the preceding schemes, electron momentum spread and beam emittance have been concluded to be major obstacles in the realization of X-ray FEL.

In an attempt to overcome the adverse effects of electron spread on short-wavelength gain, the notion of lasing without inversion (LWI) (17) in atomic systems, namely, the cancellation of absorption by interference in the gain medium, has recently been proposed for FELs (18). These proposed schemes involve a two-wiggler FEL, which bears a limited resemblance to an optical klystron (13). Unlike an optical klystron, bunching resulting from the first wiggler is reversed and the electrons are given a shift of their phase relative to the ponderomotive potential so as to cancel absorption. In the resulting gain curve, the absorption part below resonance is eliminated, whereas the gain part remains intact. Whereas in an ordinary FEL population inversion of electrons in the momentum domain is required to ensure net gain from a momentum distribution, in the proposed schemes the net gain is obtainable even from a very broad ("inhomogeneous") momentum distribution without population inversion. This creates new possibilities for development of X-ray FELs.

ELECTRON KINEMATICS: RESONANCE AND SYNCHRONISM CONDITIONS

Quantum kinematics gives a more intuitive view of the FEL gain. An electron enters the interaction region in the initial state $|\mathbf{k}_i\rangle$ and energy (the curve in Fig. 3)

$$E_i \equiv \gamma_i mc^2 = \sqrt{p_i^2 c^2 + m^2 c^4} \tag{3}$$

where the momentum $\mathbf{p} = \hbar\mathbf{k}$.

After absorption (emission) the electron has momentum $\hbar\mathbf{k}_a$ ($\hbar\mathbf{k}_e$), which is related to the energy E_a (E_e) as in Eq. (3). There is a mismatch of the longitudinal projection of these momenta from the ones obtained from the momentum conservation (see Fig. 3)

$$\Delta_e = k_{iz} - k_{ez} - k_{Lz} - k_W \tag{4}$$

$$\Delta_a = k_{az} - k_{iz} - k_{Lz} - k_W \tag{5}$$

As the interaction is considered to be stationary, i.e., not bounded in time but happening in a finite region of space, the energy is conserved precisely $E_{a,e} = E_i \pm \hbar\nu$, but the momentum admits some uncertainty given by the wiggler length L_W

$$\hbar\Delta_L \sim \frac{\hbar}{L_W} \tag{6}$$

Momentum and energy transfer k_L and $\nu = k_L c$ from light in vacuum (tilted line in Fig. 3) do not bring the final state to the dispersion curve of kinematically allowed states and, thus, cannot even approximately satisfy the conservation laws because the speed of light is larger than the electron group velocity v. Therefore, a wiggler with k_W or a medium with refractive index n, which modifies the light dispersion to $n\nu = ck_L$, is needed for either emission or absorption to happen.

We decompose the variation of energy $\hbar\nu$ with momentum in terms of a Taylor series in $\hbar(k_{az} - k_{iz})$. To this end we first approximate the dispersion curve by a straight line with the slope equal to the initial z-component of the electron velocity v

$$\Delta_a^{(0)} = \Delta_e^{(0)} = \Delta_0 = \frac{\nu}{v} - k_{Lz} - k_W \tag{7}$$

In this quasi-classical approximation the detunings for emission and absorption coincide, where emission and absorption cancel each other and there is no gain. The condition of zero detuning correspond to resonance, at which momentum is conserved precisely. It coincides with the synchronism condition, that $v = v_r$.

For a magnetostatic wiggler it generalizes the expression (1) by replacing k_L to k_{Lz}. For a Čerenkov wiggler, it yields the usual condition for Čerenkov radiation.

$$c/v = n\cos\theta \tag{8}$$

This is the usual condition for Čerenkov radiation.

To obtain a nonzero contribution to gain, we need to take into account the curvature of the dispersion curve, to second order in the longitudinal momentum variation $\hbar(k_{az} - k_{iz})$. As the laser light propagates at an angle θ with the axis, there is a corresponding transverse variation of momentum $\hbar(k_{ax} - k_{ix})$ which must be taken into account in the same order in the expansion. Upon combining the two contributions, we obtain unequal values of detunings for emission and absorption (9)

$$\Delta_a = \Delta_0 - \Delta_R,\ \ \Delta_e = \Delta_0 + \Delta_R \tag{9}$$

$$\Delta_R = \frac{\hbar\omega^2}{2mv^3\gamma^3} + \frac{n^2\sin^2\theta\hbar\omega^2}{2m\gamma vc^2} \tag{10}$$

This difference between the emission and absorption detunings is proportional to the recoil of the electrons due to the photons. The first term in Eq. (10) comes from the longitudinal variation of momentum; the second comes from the transverse variation. In general they have the same order of magnitude. Note that the effective mass for the longitudinal motion $\mathcal{M}_{\parallel} = m\gamma^3$ is different from that for the transverse motion $\mathcal{M}_{\perp} = m\gamma$.

The ratio of the shift between the centers of the emission and absorption curves, given by Δ_R, to their width Δ_L, see Eq. (6) is

$$\frac{\Delta_R}{\Delta_L} = \epsilon\frac{2\pi^2c^3}{v^3}\left(1 + \frac{n^2\sin^2\theta\gamma^2v^2}{c^2}\right) \tag{11}$$

$$\epsilon = \frac{\lambda_c L}{\lambda^2\gamma^3} \tag{12}$$

Here $\lambda_c = \hbar/(mc) \sim 4 \times 10^{-13}$ m is the Compton wavelength of electrons. The regime of operation of the FEL is quantum, if $\epsilon \sim 1$, or classical if $\epsilon \ll 1$. The parameter ϵ reaches unit at wavelength λ_q of the order of several nanometers. Thus, because all FELs currently operate in the classical regime, classical theory is sufficient for their description. The quantum limit will be reached only by X-ray lasers. Examples of gain lineshapes in the quantum and classical regimes are shown in Fig. 2a and b, respectively.

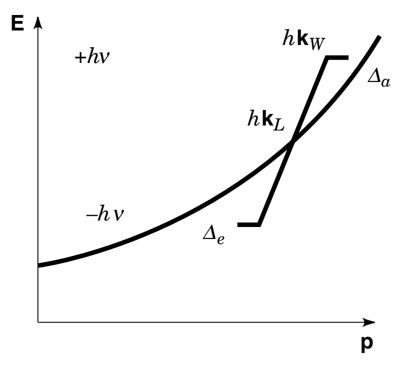

Figure 3. Energy and momentum of an electron after emission or absorption: the wiggler momentum k_W brings them close to the dispersion curve of a free electron.

CLASSICAL ELECTRON DYNAMICS

The classical dynamics of electrons in a FEL (1) is described by the Hamiltonian

$$H \equiv \gamma mc^2 = c\sqrt{(\mathbf{p} - e\mathbf{A})^2 + m^2c^2} \tag{13}$$

where m is the mass of an electron, e is the charge of an electron, c is the velocity of light, γ is referred to as the Lorentz factor, $\mathbf{p}$ is the canonical momentum, and $\mathbf{A} = A_W + A_L$ is the vector potential of the combined field of the wiggler, oriented along the z-axis (designated by subscript W), and the laser field (designated by subscript L), which propagates at an angle θ to the axis of the wiggler, i.e., has the wavector $\mathbf{k}_L = (\mathbf{k}_L \sin\theta, 0, \mathbf{k}_L \cos\theta)$, as in Fig. 1. Both fields are y polarized, and ϕ is the phase of the laser field at the instant of the electron entry into the wiggler.

$$\mathbf{A}_W = \hat{\mathbf{y}}A_W \cos(k_W z) \tag{14}$$

$$\mathbf{A}_L = \hat{\mathbf{y}}A_L \cos(-\nu t + k_L z\cos\theta + k_L x\sin\theta + \phi)] \tag{15}$$

The magnetic field of the wiggler and the electric field of the laser are

$$\mathbf{B}_W = \nabla \times \mathbf{A}_W,\ \mathbf{E}_L = -\frac{\partial}{\partial t}\mathbf{A}_L \tag{16}$$

and $\hat{\mathbf{y}}$ is the unit vector along the y-axis, and ϕ is the phase of the laser field at the instant of the electron entry into the wiggler. Dimensionless potentials (with $j = L, W$) are

$$a_j = \frac{eA_j}{\sqrt{2}mc} \tag{17}$$

Just like any other laser, FEL can operate in multimode regime. Here we consider only a single-mode field. For details about the mode competition see (19).

Hamilton equations determine the derivatives of energy and momenta

$$\frac{d\gamma mc^2}{dt} = \frac{\partial H}{\partial t},\ \frac{dp_x}{dt} = -\frac{\partial H}{\partial x},\ \frac{dp_z}{dt} = -\frac{\partial H}{\partial z} \tag{18}$$

The Hamiltonian does not depend explicitly on y; therefore, if the initial value of the momentum along y is $p_y(0) = 0$, it remains zero at all times $p_y(t) = 0$. Then the wiggling motion in this direction is described by the y component of the velocity

$$\frac{dy}{dt} = \frac{\partial H}{\partial p_y} = \frac{-eA_y}{\gamma m} \equiv v_y \tag{19}$$

For the other coordinates

$$\frac{dz}{dt} = \frac{\partial H}{\partial p_z} = \frac{p_z}{\gamma m} \equiv v_z,\ \frac{dx}{dt} = \frac{\partial H}{\partial p_x} = \frac{p_x}{\gamma m} \equiv v_x \tag{20}$$

In the Hamilton equations substituting these equations back into Eq. (13) we obtain a useful relation

$$1 = \frac{v^2}{c^2} + \frac{1}{\gamma^2} \tag{21}$$

From now on we consider ultrarelativistic electrons ($\gamma \gg 1$, i.e., $v \approx c$). There are terms of interaction with the fields having various dependences on the time and the coordinates. Of those, following a standard procedure (19), we drop (in an analog of the rotating wave approximation) the terms that are rapidly oscillating in the frame of reference of an electron moving with the injected velocity v_i close to c. The remaining ("near-resonant") terms oscillate slowly in this frame of reference. Sometimes lasing occurs at frequencies corresponding to higher harmonics of the electron wiggling motion. This corresponds to the wiggler field into higher powers, see (1). In this way we obtain the equations of motion for the energy and momenta

$$\frac{d\gamma}{dt} = \mathcal{N}\sin(-\nu t + q_z z + q_x x + \phi) \tag{22}$$

$$\frac{mc^2}{\nu}\frac{d\gamma}{dt} = \frac{1}{q_z}\frac{dp_z}{dt} = \frac{1}{q_x}\frac{dp_x}{dt} \tag{23}$$

where

$$\mathcal{N} = \frac{e^2 2A_W A_L \nu}{m^2c^2\gamma_r} \tag{24}$$

The argument of the sine in Eq. (22) is the phase relative to the ponderomotive potential,

$$\psi = -\nu t + q_z z + q_x x + \phi \tag{25}$$

Equation (23) expresses the relation between the momentum transfer to the ponderomotive potential ($q_x = k_L \sin\theta$, $q_z = k_L \cos\theta + k_W$) and the corresponding energy transfer ($\nu = k_L c$).

The dynamical equations simplify in the case in which electron energies γ do not differ much from either the injected energy γ_i or the resonant energy γ_r and the longitudinal coordinate and velocity differ by a small amount from uniform motion with the injected velocity, $z = v_i t + \delta z$ and $v_z = v_i + \delta v_z$. The equation of motion becomes

$$\frac{d\gamma}{dt} = \mathcal{N}\sin(\Omega t + q_z\delta z + q_x x + \phi) \tag{26}$$

Here

$$\Omega = q_z v_{zi} - \nu \equiv q_z(v_{zi} - v_r) \tag{27}$$

is the detuning of an electron from the resonance with the ponderomotive potential, and

$$v_r = \frac{\nu}{q_z} \tag{28}$$

is its velocity corresponding to the resonant energy γ_r. Neglecting the lasing field compared to the wiggler field, we obtain that the average square of the transverse velocity is

$$\langle v_y^2 \rangle = \frac{a_W^2 c^2}{\gamma^2} \tag{29}$$

The equations for the velocity components are

$$\frac{dv_2}{dt} \approx (1 + a_W^2)\frac{q_z c^2}{\nu\gamma_r^3}\frac{d\gamma}{dt} \tag{30}$$

$$\frac{dv_x}{dt} = \frac{q_x c^2}{\nu\gamma_r}\frac{d\gamma}{dt} \tag{31}$$

These equations demonstrate that there is a one-to-one correspondence between the increment of each velocity component and the change of energy. These equations, although describing a two-dimensional motion, result in the one-dimensional pendulum equation for the phase ψ

$$\ddot{\psi} = \frac{\mathscr{P}}{\mathscr{N}}\sin\psi \tag{32}$$

$$\psi(0) = \phi \tag{33}$$

$$\dot{\psi}(0) = \Omega \tag{34}$$

$$\mathscr{P} = \frac{c^2}{\gamma_r^3\nu}(\gamma_r^2 q_x^2 + q_z^2)(1 + a_W^2) \tag{35}$$

Small-Signal Small-Gain Regime

In general, gain produced by electrons with a well-defined initial energy or longitudinal velocity v_z (homogeneous gain)

$$G_{\text{hom}}(v_z) = -\frac{Jmc^2}{eI_L S_L}\langle\Delta\gamma\rangle \tag{36}$$

where J is the current in the electron beam, $I_L = \epsilon_0 c\nu^2 A_L^2/2$ is the intensity of the laser, S_L is the effective area of the laser mode, and the average over the uncontrollable injection phase is designated by $\langle. \ . \ .\rangle$. In the small-signal approximation, one assumes the laser vector potential being much smaller than the wiggler vector potential. For the effects of a large laser field amplitude ("large-signal gain," or "saturation") see (2). In the small-gain approximation one disregards the effect of the change in the laser field as it propagates through the wiggler on the electron dynamics. In the case of electrons distributed over v_z with a normalized distribution function $f(v_z)$, the inhomogeneous $G_{\text{inh}}(v_v)$ gain is the convolution of f and G_{hom}.

An analytical expression for the gain in the small-gain small-signal regime for a uniform wiggler can be obtained by solving the foregoing equations in a perturbation series in the laser amplitude (in the small parameter $\mathscr{N}2T$). The travel time in the wiggler $T = L_W/v_r$. For the effects of a large laser field amplitude ("large-signal gain," or "saturation"), see Ref. 2.

To zeroth order the coordinates δz and x vanish, which yields

$$\frac{d\gamma^{(1)}}{dt} = \mathscr{N}\sin(\Omega t + \phi) \tag{37}$$

When averaged over injection phases, the net change of the energy (and consequently gain) is zero to this order.

To first order in the lasing amplitude, the coordinates are from Eq. (25)

$$\delta z^{(1)}(t) = \frac{q_z c^2}{\nu\gamma_r^3}\int_0^t \Delta\gamma^{(1)}(t')\,dt' \tag{38}$$

$$x^{(1)}(t) = \frac{q_x c^2}{\nu\gamma_r}\int_0^t \Delta\gamma^{(1)}(t')\,dt' \tag{39}$$

Expansion of Eq. (26) around the solution of Eq. (37) with the forementioned coordinates gives

$$\frac{d\gamma^{(2)}}{dt} = \mathscr{P}\mathscr{W}\cos(\Omega t + \phi)\int_0^t \Delta\gamma^{(1)}(t')\,dt' \tag{40}$$

When integrated over interaction time T and averaged over the injection phases, the change of energy and, consequently, gain, is nonzero in this order

$$\begin{aligned}\langle\Delta\gamma^{(2)}\rangle &= \frac{\mathscr{P}\mathscr{W}^2}{2\Omega^3}[\Omega T\sin\Omega T + 2\cos\Omega T - 2] \\ &\equiv T^3\mathscr{P}\mathscr{W}^2\frac{1}{8}\frac{d}{d\alpha}(\text{sinc}^2\alpha)|_{\alpha=\Omega T/2} \equiv -G_{st}(\Omega, T)\end{aligned} \tag{41}$$

This gives a gain lineshape similar to that in Fig. 2b. The relative width of the gain curve is

$$\frac{\Delta\nu}{\nu} = \frac{\Delta\gamma}{\gamma} \approx \frac{1}{2N_W} \tag{42}$$

where N_W is the number of wiggler periods, $L_W = N_W\lambda_W$. The derivative over the detuning parameter in Eq. (41) is the manifestation of a more general Madey theorem (12)

$$\langle\Delta\gamma^{(2)}\rangle = \frac{\partial}{\partial\gamma_i}\langle(\Delta\gamma^{(1)})^2\rangle \tag{43}$$

where the left-hand side is proportional to gain and the expression under the derivative in the right-hand side is proportional to the energy spread; γ_i is the initial Lorentz factor. The theorem holds for the Hamiltonian motion of a particle in a weak oscillating perturbation (i.e., small-signal, small-gain regime for FELs). It can be shown that the energy spread is proportional to the power of spontaneous emission. The Madey theorem simplifies the calculation of gain in nonuniform wigglers.

A compact expression for gain per pass is obtainable for $\theta = 0$ by combining Eq. (41) with Eqs. (2) and (28)

$$G_{st} = -\frac{\pi^2 N_W^3 a_W^2}{\gamma_r^3}\frac{\lambda_W^2}{S_L}\frac{J}{J_A}\frac{d}{d\alpha}(\text{sinc}^2\alpha) \tag{44}$$

Here $J_A = ec/r_0$ is the Alfven current and r_0 is the classical electron radius. We see that gain rapidly decreases with the increase of γ_r, which adds difficulty to achieving short-wavelength lasing.

DYNAMICS AND GAIN IN INTERFERING TWO-WIGGLER FELS

To focus on the effects of interference of coherent radiation processes, we will consider the interaction in two identical

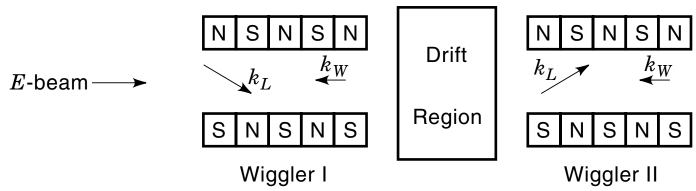

Figure 4. A scheme of realization of a two-wiggler FEL with a drift region between wigglers.

wigglers of length L_W with a dispersive drift region of length L_d between them (20) (Fig. 4). Electrons can be guided in the drift region by magnetic field; light can be deflected by mirrors. The effect of the drift region is an addition of phase delay $\Delta\psi$ in the second wiggler relative to the first one, which, on examining Eq. (25), is seen to be

$$\Delta\psi = k_L\left(s_L - \frac{s_e(v)c}{v} + x_{II}\sin\tilde{\theta} - x_I\sin\theta\right) \tag{45}$$

where $s_e(v)$ denotes the velocity-dependent electron paths and s_L denotes the lightwave paths in the drift region, $\tilde{\theta}$ is the angle of propagation of the laser in the second wiggler and θ is the angle in the first wiggler, x_I and x_{II} are the transverse coordinates at the exit from the first wiggler and at the entrance to the second wiggler, and v is the absolute value of the electron velocity, which is not changed in the drift region.

The electron oscillates coherently in the ponderomotive potential and, therefore, its oscillations in the two sequential wigglers exhibit interference that depends on the path (or time) difference between the two regions.

Then the change of energy in the second wiggler is given by

$$\frac{d\gamma_{II}^{(1)}}{dt} = \mathscr{N}\sin(\Omega t + \phi + \Delta\psi) \tag{46}$$

$$\frac{d\gamma_{II}^{(2)}}{dt} = \mathscr{P}\mathscr{W}\cos(\Omega t + \phi + \Delta\psi)\int \Delta\gamma^{(1)}\,dt' \tag{47}$$

Application of Eqs. (40) and (47) yields the phase-averaged energy change in the whole FEL

$$\begin{aligned}\langle\Delta\gamma^{(2)}\rangle = {} & \frac{\mathscr{P}\mathscr{W}^2}{2\Omega^3}[2\Omega T\sin\Omega T + 4\cos\Omega T - 4 \\ & + 2\Omega T\sin(2\Omega T + \Delta\psi) - 2\Omega T\sin(\Omega T + \Delta\psi) \\ & + 2\cos\Delta\psi + 2\cos(2\Omega T + \Delta\psi) - 4\cos(\Omega T + \Delta\psi)]\end{aligned} \tag{48}$$

For the case of a usual FEL ($\Delta\psi = 0$), this gives the well-known expression $-G_{st}(\Omega, 2T)$.

In the case of the optical klystron, the propagation angle in the first wiggler $\theta = 0$, and the light goes straight $s_L = L_d$. If there is just a transverse magnetic field A_y in the drift region, the slope of the electron trajectory is

$$\frac{dy}{dz} = \frac{eA_y}{\gamma m v_z} \tag{49}$$

Then for a small slope

$$\frac{ds_e}{dv_z} \approx \frac{L_d - s_e}{v_z} \tag{50}$$

and, with or without the magnetic field in the drift region, the change of phase grows with velocity, $d\psi/dv_z > 0$. Gain of an optical klystron for $\Delta\psi = 5\Omega T$ is shown in Fig. 5. The peak gain can greatly increase compared to that of the usual FEL, but the width of the peak decreases and the whole curve remains an odd function of Ω.

The problem with conventional classical interference in an optical klystron, is that it does not distinguish between electrons that emit or absorb energy. The total phase delay, from the entrance to the first wiggler to the entrance to the second one, remains strongly dispersive (velocity-dependent) and the resulting gain is sensitive to the initial velocity spread. In Ref. (20) we have pursued the following radically new approach to classical interference: (1) the electron beam is separated after the first region into two components whose velocities correspond to either absorption or emission (on the average) in the first region; and (2) each of the separated components is given different phase delays that compensate for the velocity spread in Ω. These phase delays ensure both the cancellation of the absorption contributions in the two regions and the doubling of the emission counterparts over a wide range of velocities.

To compensate for velocity dispersion, we wish to impose the following phase delay on the beam component, which contributes to emission (with $\Omega > 0$, i.e., $v_{iz} > v_r$), up to the moment it enters the second region

$$\Delta\psi(\Omega > 0) = 2\pi N - q_z(v_z - v_r)T \tag{51}$$

where N is an integer. The electrons with $\Omega < 0$ that have absorbed (on the average) energy in the first region must undergo the same function of the phase shift as in Eq. (51), except for an extra phase π

$$\Delta\psi(\Omega < 0) = (2N+1)\pi - q_z(v_z - v_r)T \tag{52}$$

Note that $\Delta\psi$ depends on the velocity at the entrance to the first wiggler rather than the exit from it. For such a situation, the Madey theorem applies only in a modified form.

To implement such a delay function, let us examine more closely the velocity changes in the first wiggler. From Eqs. (30) and (31) we find

$$\frac{dv_x}{dv_z} = \frac{q_x\gamma_r^2}{q_z} \approx \gamma_r^2\sin\theta \tag{53}$$

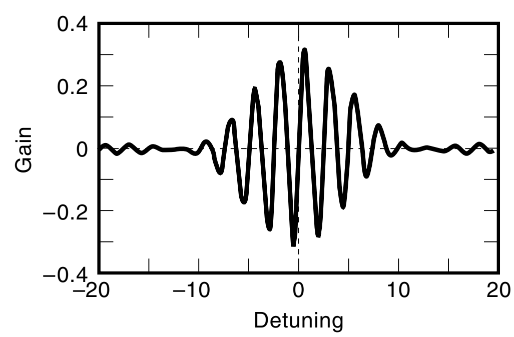

Figure 5. Gain in an optical klystron as a function of detuning. Peak gain is higher.

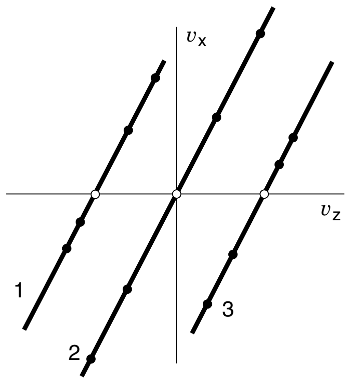

Figure 6. Changes of the transverse and the longitudinal velocities are proportional. Open dots—initial states, closed dots—final states.

the approximate equality corresponding to a small angle θ and $k_L \gg k_W$.

The amount of velocity change is determined by the detuning and the injection phase, but the changes of the v_z and v_x velocity components are proportional to each other. Integrating Eq. (53), we see that

$$v_x = \gamma_r^2 \sin\theta (v_z - v_{zi}) \tag{54}$$

Hence the transverse velocity after the first wiggler is correlated to the change in the longitudinal velocity. It is thus possible to distinguish by their v_x value those electrons that experienced net emission from those that experienced net absorption.

As seen from Fig. 6, electrons with initial velocity below resonance ($v_{zi} < v_r$) end up in the half-plane above the line

$$v_x = \gamma_r^2 \sin\theta (v_z - v_r) \tag{55}$$

Electrons with initial velocity higher than the resonant one ($v_{zi} > v_r$) are now below this line. Then the step-like change in the phase delay from 0 to π needs to be arranged along this line, as it is shown in Fig. 7.

The electrons will enter the drift region at different angles depending on their transverse velocity. By their deflection in a magnetic field, they will receive a phase delay corresponding to $-q_z(v_z - v_r)T$, the smooth part of the delay function [see Eq. (51)]. In addition, the electrons with v_x of that in Eq. (55) will be sent to a region of magnetic field with sharp boundaries, where they travel on additional path corresponding to the phase π. This implements the step-like part of the phase delay of Eq. (52).

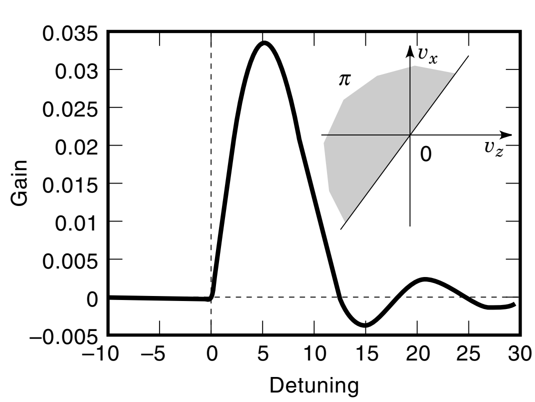

Figure 7. The implementation of FELWI using both longitudinal and transverse components of the velocity (upper right-hand corner); numerical result for the gain; $\mathcal{N}2T = 0.03$.

When the selective phase delay, determined by Eqs. (51) and (52), is used in the expression for gain Eq. (48), it results indeed in cancellation (destructive interference) of the absorptive contributions from the two regions and addition (constructive interference) of their emission counterparts

$$G_{FELWI}(\Omega, 2T) = 4G_{\mathrm{st}}(\Omega, T)\Theta(\Omega) \tag{56}$$

where Θ is the Heaviside step function.

This gain function, which is positive nearly everywhere, essentially does not require population inversion and yields gain even from broad inhomogeneous distributions (Fig. 7). We therefore designate it as FEL without inversion (FELWI).

Field Dynamics in Large-Gain Regime

Up to now only the small-gain regime (neglecting the change of laser field) of FEL was considered. We describe the variation of the laser field by Maxwell's equations for the transverse part of the field

$$\left(\nabla^2 - \frac{1}{c^2}\frac{\partial^2}{\partial t^2}\right) A_y = -\mu_0 J_y \tag{57}$$

where the transverse current density is

$$J_y = e\sum_j v_y \delta(\mathbf{x} - \mathbf{x}_j(t)) \tag{58}$$

Here the sum runs over all electrons and v_y is obtained from (19). We write the equations only for phasors of the vector potentials

$$A_{Wy} = A_W(z)\exp(ik_W z) \tag{59}$$

$$A_{Ly} = A_L(z', t)\exp(-i\nu t + ik_L z' + i\phi) \tag{60}$$

We make the slowly-varying envelope approximation, i.e., assume that $A_L(z', t)$ varies little over a wavelength or the time period of optical oscillations in the direction of propagation $z' = z\cos\theta + x\sin\theta$. In this approximation one neglects the second derivatives of the envelope. Besides, the right-hand side should also be averaged (designated by $\langle . \ . \ . \rangle$) over several wavelengths, which reduces to the above averaging over ϕ for a constant envelope. Thus (57) becomes

$$\left(\frac{\partial}{\partial z'} + \frac{1}{c}\frac{\partial}{\partial t}\right) A_L = \frac{\omega_p^2}{2ic\nu}\left[A_W\left\langle\frac{e^{-i\psi}}{\gamma}\right\rangle + A_L\left\langle\frac{1}{\gamma}\right\rangle\right] \tag{61}$$

where the plasma frequency

$$\omega_p^2 = \frac{e^2 n}{\epsilon_0 m} \tag{62}$$

and n is the density of electrons.

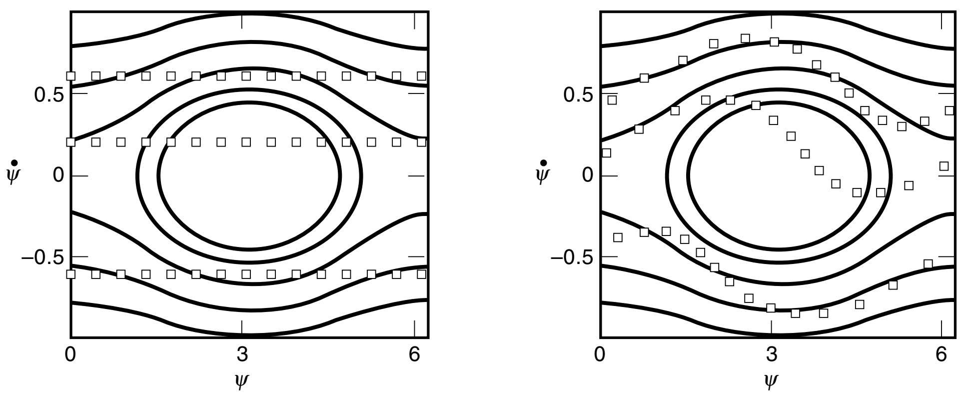

Figure 8. Motion of electrons in the coordinates ψ, $\dot{\psi}$ of the pendulum.

If the density is high, we need to correct the equation of motion for the electrons for the electric field created by a nonuniform charge distribution, following (4)

$$\frac{d\gamma}{dt} = \frac{2\omega_p^2}{\nu}(\langle\cos\psi\rangle\sin\psi - \langle\sin\psi\rangle\cos\psi) \tag{63}$$

The dimensionless parameter (4)

$$\rho = \frac{1}{\gamma}\left(\frac{a_W\omega_p}{4ck_W}\right)^{2/3} \tag{64}$$

is the indicator whether the plasma effects due to Coulomb interaction between electrons are important ($\rho \gtrsim 1$, called "Raman regime") or whether one can consider electrons interacting directly with the field only ($\rho \ll 1$, called "Compton regime").

One can see from the pendulum Eqs. (32–35) that if the change of the laser field is small, the gain will saturate when the electrons will make about one cycle in the pendulum coordinates, i.e., $\mathscr{P}\mathscr{N}T^2 \sim \pi^2$. To offset this effect, tapered wigglers (with variable wiggler wavelength and/or field) are used (2).

Even in the Compton regime, light emission can be collective. If the gain is large enough, the electrons bunch in the pendulum coordinates and correspondingly in space over the length of order of λ_L, see Fig. 8. This is expressed as a nonzero average phase factor $\langle e^{i\psi}\rangle$. The field adjusts its phase so as to cause the bunched electrons to give even more energy to the field. Thus the gain is much larger than expected from a small-gain analysis in Section III. This collective effect corresponds to superradiant emission. Description in terms of collective variables, such as bunching, is sometimes possible (4).

FELWI Versus Ordinary FEL in the Large-Gain Regime

We can solve numerically the set of Eqs. (32–35) together with Eqs. (61) and (63) to investigate the electron beam behavior and the gain in a large-gain FEL. They will be compared to their counterparts in a large-gain FELWI, using the scheme of Sec. IV.

To this end, we substitute

$$\frac{d}{dt} \to v_r\frac{\partial}{\partial z} + \frac{\partial}{\partial t} \tag{65}$$

and calculate the space dependence of the field and beam parameters. We will vary the dimensionless size of the wiggler $\tilde{L}_W = 2k_W\rho L_W$ (which corresponds to either the change of the current of electron beam or the length of the wigglers).

Numerical results for the monoenergetic beam can be checked against the available analytical ones in the small-signal small-gain regime. Figure 9 shows the comparison of the results obtained by a computer simulation for the ordinary FEL and for the FELWI.

For a small a current ($\tilde{L}_W = 0.5$) the results practically coincide with analytical calculations (20), namely, the integral over detunings equals to zero for the ordinary FEL, but is nonzero for the FELWI. At a slightly higher current ($\tilde{L}_W = 1$) the nonzero integral over detuning appears for an ordinary FEL as well due to a nonlinear synchronization of the electron bunching and the phase of the ponderomotive potential. We see that the peak gain for an ordinary FEL is higher than for FELWI, but this situation is reversed in the large-signal regime.

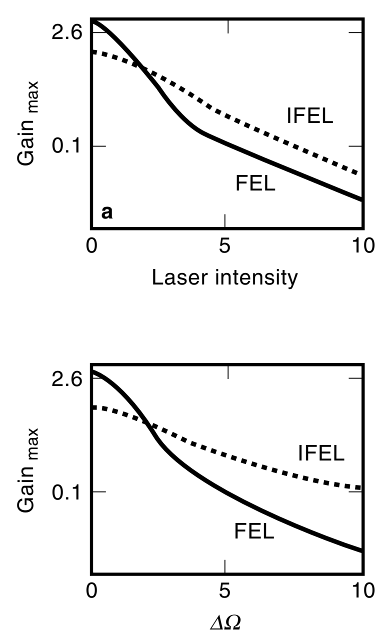

Figure 9. The dependence of maximum gain on the laser field intensity (a) and on the width of electron spread (b) for the ordinary FEL (solid line) and for the FELWI (dashed line). Wiggler length, $\tilde{L}_W = 1$.

The dependence of gain on the laser field intensity is very important because it determines maximum laser intensity. As the laser intensity grows, the electrons perform more than one revolution in their pendulum-like phase space, and start contributing negatively to gain. This decrease of the net gain is referred to as saturation. In Fig. 9(a), we present the dependence of maximum gain on the laser intensity for the IFEL and the FEL. It is clearly seen that only for small intensities of the laser field does the FEL gain exceed that of the IFEL. As the laser intensity grows, the IFEL gain exceeds that of an ordinary FEL. That means that an IFEL promises a higher saturated laser intensity.

Let us assume that the electron momentum distribution in Gaussian with mean value Ω_c and variance $\Delta\Omega_{el}$. In Fig. 9(b), we present the dependence of the maximum gain on the width $\Delta\Omega_{el}$ of the electron momentum spread. The maximum gain for an ordinary FEL dramatically drops with the increase of $\Delta\Omega_{el}$, and we can remark that even for a large $\tilde{L}_W$ small-gain regime conditions are valid. The maximum gain drops much faster for the ordinary FEL, namely,

$$(G_{\max})_{\text{FEL}} \sim \frac{1}{\Delta\Omega_{\text{el}}^2} \tag{66}$$

than for a FELWI

$$(G_{\max})_{\text{FELWI}} \sim \frac{1}{\Delta\Omega_{\text{el}}} \tag{67}$$

Thus we can conclude from the preceding considerations that, due to absorption cancellation at negative detunings, the FELWI has a higher gain for the electron beam with a spread of momentum; this gives us a powerful way to extend the FEL to the short-wavelength region up to VUV and X-ray.

QUANTUM REGIME OF FEL

In order to calculate the emission and absorption amplitudes quantum mechanically, the phasor of the vector potential in the magnetostatic wiggler (59,60), is used in its time-independent form. Likewise, in the Cerenkov wiggler, where the index of refraction periodically changes along the axis, we use the time-independent electromagnetic vector potential

$$\mathbf{A}_L = \hat{e}\sum_{j=0}^{\infty} A_{Lj} \exp[i(\mathbf{k}_L + j\mathbf{k}_W)\mathbf{r}] \tag{68}$$

where $\hat{\mathbf{e}} = (\cos\,\theta,\, 0,\, -\sin\,\theta)$, and the harmonics are determined by the inverse period of index variation $\mathbf{k}_W$, with amplitudes A_{Lj}. We will consider only the first harmonic for simplicity.

The amplitudes for emission and absorption can then be written in the general form (9)

$$\begin{aligned} T_e &= \langle \mathbf{k}_e| - \frac{e\mathbf{A}_L^*}{m\gamma}(\mathbf{p} - e\mathbf{A}_W^*)|\mathbf{k}_i\rangle \\ T_a &= \langle \mathbf{k}_a| - \frac{e\mathbf{A}_L}{m\gamma}(\mathbf{p} - e\mathbf{A}_W)|\mathbf{k}_i\rangle^* \end{aligned} \tag{69}$$

Here $|\mathbf{k}_i\rangle$ is a quantum state of an electron normalized in the volume V, and the momenta and energies of electrons before and after emission or absorption are as in Section I. The second term in the brackets is applicable in a magnetostatic wiggler, and the first term in a Čherenkov wiggler.

Gain is proportional to the difference between the squares of the foregoing two expressions. The emission amplitude in an interaction region of length L_W is given by the integral (which we take to extend to infinity in the transverse directions)

$$\begin{aligned} T_e &= \frac{eA_L^*}{m\gamma V}\int_0^{L_W} \exp(-i\mathbf{k}_e\mathbf{r})\exp(-i\mathbf{q}_j\mathbf{r})\hbar\hat{\mathbf{e}}\cdot\mathbf{k}_i\exp(i\mathbf{k}_i\mathbf{r})\,d^3\mathbf{r} \\ &= \frac{eA_{Lj}^*\hbar k_i\sin\theta}{m\gamma L}\delta(k_{ix}-k_{ex}-q_x)\delta(k_{iy}-k_{ey}-q_y) \\ &\quad \int_0^{L_W}\exp[i(k_{ix}-k_{ez}-q_{jz})z]\,dz \\ &\sim C^*\frac{\exp(i\Delta_e L)-1}{\Delta_e L} \end{aligned} \tag{70}$$

and, analogously, the amplitude for absorption is given by

$$T_u \sim C^*\frac{exp(i\Delta_a L)-1}{\Delta_a L} \tag{71}$$

Here we introduced the detunings and the coupling constant

$$\Delta_e = k_{iz} - k_{ez} - q_{jz},\ \Delta_a = k_{az} - k_{iz} - q_{jz} \tag{72}$$

The coupling constant

$$C = \frac{eA_{L1}\hbar k_i\sin\theta}{m\gamma} \qquad \text{(Čerenkov)} \tag{73}$$

For the magnetostatic wiggler, only the coupling constant changes

$$C = \frac{e^2A_LA_W}{m\gamma} \qquad \text{(magnetostatic)} \tag{74}$$

Hence, the probabilities of emission and absorption are

$$M_e(\Delta_e) = |C|^2\text{sinc}^2\left(\frac{\Delta_e L}{2}\right) \tag{75}$$

$$M_a(\Delta_a) = |C|^2\text{sinc}^2\left(\frac{\Delta_a L}{2}\right) \tag{76}$$

where

$$\text{sinc}(x) = \frac{\sin(x)}{x} \tag{77}$$

The standard homogeneous quantum gain G_{qst} is proportional to the difference between the emission and absorption rates,

$$G_{\text{qst}} \propto \text{sinc}^2(\Delta_e L/2) - \text{sinc}^2(\Delta_a L/2) \tag{78}$$

where $\Delta_{e(a)}$ is determined by Eq. (4) and Fig. (3). In the limit of small recoil (small difference beween Δ_a and Δ_e) it has the

Table 1. Parameters of Some of the First FELs

Location	Type	λ_W, cm	N	a_W	γ	I, W	λ_L, μm
Stanford	Superconducting, RF linac	3.3	160	0.71	85	2.6	3.4
TRW/Stanford	Permanent, RF linac	3.6	153	0.97	130	2.5	1.6
Novosibirsk	Klystron, storage ring	6.9	22	2.7	686	7	0.62
Orsay	Klystron, storage ring	7.8	17	2	432	1.3	0.463–0.655
Santa Barbara	Permanent, electrostatic	3.6	160	0.11	6.8	1.25	400
Livermore	Permanent, induction linac	9.8	30	2.5	6.9	850	8700
Frascati	Electro-pulsed, microtron	2.4	50	1	42	2.4	10.6
Los Alamos	Permanent, RF linac	2.73	37	0.56	43	50	10
Boeing	Permanent, RF linac	2.2	229	1.3	223	100	0.5

same lineshape as in Fig. 2b. The gain can be approximated by

$$G_{\mathrm{qst}} \approx \frac{\partial}{\partial \Delta} M(\Delta) \tag{79}$$

which is a restatement of the Madey theorem. The gain profile in Eq. (78) is almost antisymmetric about $\Delta = 0$, resulting in a very weak gain for a broad, nearly symmetric electron distribution $f(\Delta)$.

FEL EXPERIMENTAL PARAMETERS

Parameters for a set of early experiments on FELs are collected in Table 1. Here I_W is the average output power of the laser. Other parameters are defined in the text. The second column in Table 1 shows the type of the wiggler and the source of electrons. Usual sources of the electron beam are a linear accelerator (RF linac), Fig. 10, or a storage ring. Sometimes RF recovery is used in a storage ring to restore the energy of electrons.

APPLICATIONS

Free electron lasers have numerous applications. Due to their wide tunability and at the same time high peak power, they are used in precision and nonlinear spectroscopy (especially in infrared (IR) and UV regions) for the purposes of condensed matter physics and chemistry. Other uses include medical and surgical applications, microcircuit fabrication, material processing, and directed energy weapons. For a review see Refs. 1–3.

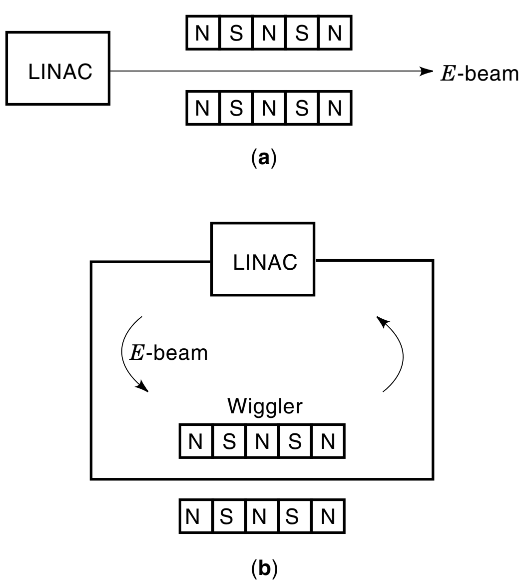

Figure 10. A scheme of realization of a linac (a) and a storage ring (b).

PERSPECTIVES

The main direction of further development of FELs will probably be in the achievement of an X-ray wavelength via the large-gain regime (4). As a result, the problems of electron energy spread and emittance will have to be solved. Theoretical constructs of a collective atomic recoil laser (21) are expected to bridge the gap between the usual lasers and FELs. Studies on optimization of a conventional FEL design (see, for example, Ref. 22), including the effects of saturation and FEL geometry, are also underway at this time.

BIBLIOGRAPHY

1. C. A. Brau, *Free Electron Lasers,* New York: Academic Press, 1990.
2. P. Luchini and H. Motz, *Undulators and Free-Electron Lasers,* Oxford: Clarendon, 1990.
3. G. Dattoli, A. Renieri, and A. Torre, *Lectures on the Free Electron Laser Theory and Related Topics,* London: World Scientific, 1993.
4. R. Bonifacio, C. Pellegrini, and L. Narducci, *Opt. Commun.,* **50**: 373, 1984; R. Bonifacio et al, *Revista del Nuovo Cimento,* **13**: 1, 1990.
5. D. F. Alferov, Yu. A. Bashmakov, and P. A. Čerenkov, *Sov. Phys. Usp.,* **32**: 200, 1989; E. G. Bessonov, A. V. Vinogradov, *Sov. Phys. Usp.,* **32**: 806, 1989.
6. J. M. Madey, *Jour. Appl. Phys.,* **42**: 1906, 1971.
7. F. A. Hopf et al., *Opt. Commun.,* **18**: 413, 1976; *Phys. Rev. Lett.,* **37**: 1342, 1976.
8. W. B. Colson, *Phys. Lett.,* **59A**: 187, 1976.
9. A. Friedman et al., *Rev. Mod. Phys.,* **60**: 471, 1988.
10. D. A. G. Deacon et al., *Phys. Rev. Lett.,* **38**: 892, 1977.
11. P. Dobiash, P. Meystre, and M. O. Scully, *IEEE J. Quant. Electr.,* **QE-19**: 1812, 1983; J. Geo-Banacloche et al., *IEEE J. Quant. Electr.,* **QE-23**: 1558, 1987.
12. J. M. J. Madey, *Nuovo Cimento,* **50B** (64): 1978; N. M. Kroll, P. L. Morton, M. N. Rosenbluth, *IEEE J. Quan. Electr.,* **QE-17**: 1436, 1981.
13. N. A. Vinokurov and A. N. Skrinsky, Institute of Nuclear Physics, Novosibirsk Report No. INP77-59, 1977 unpublished; N. A. Vinokurov, *Proc. 10th Inter. Conf. on High Energy Particle Accelerators,* Serpukhov, 1977.

14. A. Gover and P. Sprangle, *IEEE J. Quant. Electr.,* **QE-17**: 1196, 1981.
15. S. Datta and A. E. Kaplan, *Phys. Rev.* A **31**: 790, 1985.
16. L. R. Elias, *Phys. Rev. Lett.,* **42**: 977, 1979.
17. O. Kocharovskaya and Y. Khanin, JETP Lett., **48**: 630, 1988; S. E. Harris, *Phys. Rev. Lett.,* **62**: 1033, 1989; M. O. Scully, S. Y. Zhu, and A. Gavrielides, *Phys. Rev. Lett.,* **62**: 2813, 1989.
18. G. Kurizki, M. O. Scully, and C. Keitel, *Phys. Rev. Lett.,* **70**: 1433, 1993; D. E. Nikonov, B. Sherman, G. Kurizki, M. O. Scully, *Opt. Commun.,* **123**: 363, 1996.
19. A. Yariv, *Quantum Electronics,* New York: Wiley, 1989, chap. 13.
20. B. Sherman et al., *Phys. Rev. Lett.,* **75**: 4602, 1995; D. E. Nikonov, M. O. Scully, and G. Kurizki, *Phys. Rev. E,* **54**: 6780, 1996.
21. R. Bonifacio et al., *Phys. Rev.* A, **50**: 1716, 1994.
22. E. L. Saldin, E. A. Schneidmiller, and M. V. Yurkov, *Phys. Rep.,* **260**: 187, 1995.

DMITRI E. NIKONOV
University of California at Santa Barbara

GERSHON KURIZKI
Max-Planck-Institut für Quantenoptik

YURI V. ROSTOVTSEV
Texas A&M University

FREE ELECTRON LASERS. See SUBMILLIMETER WAVE LASERS.

FREE FORM SURFACE RECONSTRUCTION. See FUNCTION APPROXIMATION.

FREE-SPACE PROPAGATION. See FRIIS FREE-SPACE TRANSMISSION FORMULA.

FREE-SPACE TRANSMISSION. See FRIIS FREE-SPACE TRANSMISSION FORMULA.

FREE-SPACE TRANSMISSION FORMULA. See FRIIS FREE-SPACE TRANSMISSION FORMULA.